7A52 铝合金双丝焊工艺及焊缝耐腐蚀性

解瑞军[1]， 陈芙蓉[1]， 张传臣[1]， 高云喜[2]
（1. 内蒙古工业大学 材料科学与工程学院，呼和浩特 010051；
2. 包头北方工程技术开发有限责任公司，内蒙古 包头 014033）

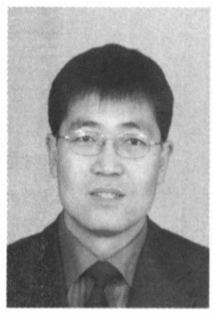

解瑞军

摘 要：采用 ER5356 焊丝对 40 mm 厚 7A52 铝合金板进行双丝气体保护焊。对母材及双丝焊焊缝显微组织进行分析，同时根据 7A52 铝合金在实际生产中的应用情况，进行了母材及焊缝在 3.5% NaCl 腐蚀溶液中的盐雾腐蚀试验。结果表明，双丝焊焊缝组织由α(Al)+β($MgZn_2$)相组成，且焊缝组织较为致密、晶粒细小、焊缝中心为等轴晶粒。7A52 铝合金母材在潮湿的含氯离子环境中容易诱发点蚀，腐蚀后的材料表面覆盖有一层致密的 Al_2O_3 氧化膜，该氧化膜可有效地延缓腐蚀的继续发展。双丝焊焊缝耐腐蚀性较好，表面点蚀较少。

关键词：7A52 铝合金；双丝焊；显微组织；耐腐蚀性
中图分类号：TG407 文献标识码：A 文章编号：0253－360X(2008)12－0057－04

0 序 言

7A52 铝合金是国内自行研制开发的一种可热处理强化的高强可焊铝合金结构材料，熔铸方便，成形性好，经轧制能获得比较理想的板材，通过适当的固溶及回归再时效处理，可使该合金获得优良的综合性能，目前已在建筑、军用设施、航空航天器与地面车辆和装备等焊接构件中获得批量应用[1,2]。但目前该类合金的焊接主要采用单丝 MIG 焊，焊后焊缝中容易出现焊接变形和气孔，残余应力较大，且对应力腐蚀敏感。单丝 MIG 焊后其焊缝性能明显下降，不能充分发挥材料的性能[2]。探索新的焊接方法在 7A52 铝合金构件材料中的应用，是非常必要和非常迫切的[3]。利用双丝焊技术焊接铝合金，可通过协调器调整各自参数，形成统一熔池，最大限度地满足电弧控制要求，从而获得满意的焊缝，提高焊接效率。文中对 7A52 铝合金母材及双丝焊焊缝组织进行了观察分析，同时根据该铝合金在水陆两用战车上的实际应用情况，考察了母材及焊缝在盐雾腐蚀试验后的微观形貌及腐蚀产物组成等，以期为该材料腐蚀机理的研究及采取相应的防护手段提供依据。

收稿日期：2008－07－11
基金项目：国家自然科学基金资助项目(50765003)

1 试验方法

试验材料选用 40 mm 厚的 Al-Zn-Mg 系 7A52 铝合金板。材料抗拉强度 $R_m \geqslant 410$ MPa，断后伸长率 $A \geqslant 7\%$。采用直径为 1.6 mm 的 ER5356 焊丝进行焊接，其主要化学成分见表 1。试验用气体为纯氩，纯度≥99.99%。

表 1 ER5356 焊丝的化学成分(质量分数，%)

Table 1 Composition of welding wire ER5356

Cu	Mn	Mg	Cr	Zn	Ti	Al
0.1	0.05～0.20	4.5～5.5	0.05～0.20	0.10	0.06～0.20	余量

双丝焊焊接设备采用奥地利 Fronius 公司生产的 TPS5000 多功能数字化焊机及与其配套的 IGM 焊接机器人等进行施焊。双丝焊接设备通过两台焊机特殊的装置进行通讯，保证两个电弧之间互不干扰，焊接铝合金采用相位差 180° 的熔滴过渡形式，以使脉冲电流相互交替作用于熔池。双丝焊机每个电源参数持续可调，且调节范围大，可以很方便地调节电源外特性，使之能够符合母材、填充金属和保护气体的要求。当焊接参数设置到最佳时，脉冲电弧能得到无短路、几乎无飞溅的过渡过程，真正做到“一个脉冲过渡一个熔滴”。其相位调节示意图如图 1 所示。

40 mm 板厚采用双面 V 形 70° 坡口，正反面各焊

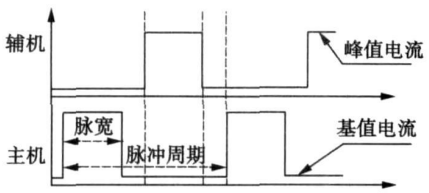

图 1 脉冲弧焊电极 1 和电极 2 的相位调节

Fig. 1 Phase regulation in electrode 1 and 2 of pulse welding

3 道。焊后各区微观组织的观察在 GX51 光学金相显微镜上进行。在 YXW 型盐雾箱进行连续盐雾腐蚀试验，腐蚀时间为 50 h，腐蚀产物的去除用 50 mL 磷酸，120 g 三氧化铬加蒸馏水配制成 1 000 mL 溶液，使用温度为 80 ~ 100 ℃，加热时间 5 ~ 10 min。并在配有 INCA Energy-Oxford 能谱仪(EDS)的 Quanta 400-FEI 扫描电镜(SEM)上进行腐蚀形貌观察。

2 试验结果及分析

2.1 显微组织分析

7A52 铝合金母材显微组织如图 2 所示，其微观组织是典型的轧制组织，经淬火与人工时效处理后，轧制组织由再结晶组织与变形的带状组织组成，化合物被破碎并沿轧制方向排列，母材组织为 α(Al)＋T($Mg_3Zn_3Al_2$)相。

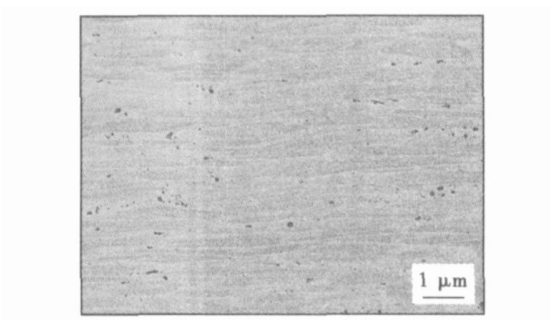

图 2 母材显微组织

Fig. 2 Microstructure of base metal

双丝焊焊缝显微组织如图 3 所示，由图可以看出焊缝组织由 α(Al)＋β($MgZn_2$)相组成，与单丝焊相比[2]，双丝焊焊缝组织较为致密，晶粒细小，这是由于双丝焊焊接速度快，热输入小的原因所致。

2.2 耐盐雾腐蚀性能

经测试，母材的失重为 0.003 55 g，腐蚀速率为 0.034 22 g/(m^2·h)。焊缝的失重为 0.003 65 g，腐蚀速率为0.02704g/(m^2·h)。为了详细比较和说明母

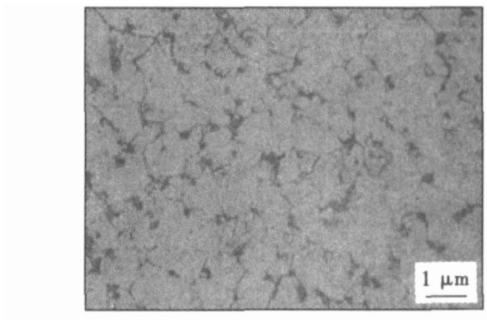

图 3 双丝焊焊缝显微组织

Fig. 3 Microstructure of double-wire welded seam

材与焊缝的腐蚀情况，用扫描电镜对其腐蚀形貌进行了观察，并对腐蚀产物中的两个典型区域，即皲裂区和白色产物区进行了相应的能谱分析。图 4 和图 5分别为母材和焊缝腐蚀产物形貌及相应的能谱分析结果。

图 4a 和图 4c 分别是对应母材不同部位的腐蚀形貌，图 4b 和图 4d 分别是对应于图 4a 中 A 区和对应于图 4c 中 B 区的能谱分析结果。

从图 4a 和图 4c 母材腐蚀形貌可以发现，在母材的基体中除有大面积的腐蚀产物外，在基体上还散布着大小不均匀的腐蚀坑，可见 7A52 铝合金基体上发生了点腐蚀。从图 4a 中还可以看出，在没有发生点蚀的部位，一层较厚的腐蚀产物膜覆盖在基体表面(其成分主要为 Al_2O_3)，且腐蚀产物膜发生了皲裂。通过图 4b 即对应图 4a 的母材 A 区能谱分析得知，该产物膜中含有少量 Cl^-，疏松的孔洞就成为 Cl^- 的活性通道，易于 Cl^- 向基体内部渗透，使腐蚀向金属内部扩展。在腐蚀产物膜上出现了大量的不规则的纵横交错的裂纹。腐蚀产物膜被这些裂纹割裂成不规则的小板块。这为基体腐蚀进一步向纵向扩展提供了可能，使基体金属容易发生点蚀。从图 4d，即对应图 4c 的母材 B 区的能谱分析可以发现，在发生点蚀的部位有白色的腐蚀产物，其中含有 Fe 元素，这说明元素 Fe 促进了点蚀的发生和继续，Fe 元素在铝合金中属于杂质，对合金的抗蚀性、力学性能及焊接性均有不利影响，所以应尽量控制其在整个基体中的含量，最好不超过 0.3%(质量分数)。

图 5a 和图 5c 分别为对应双丝焊焊缝不同部位的腐蚀形貌，图 5b 和图 5d 分别是对应于图 5a 中 C 区和对应于图 5c 中 D 区的能谱分析结果。从图 5a，5c 可以看出，双丝焊接头点腐蚀发生较少(图中规则的孔洞为焊接过程中产生的气孔。由图 5a 可以发现，双丝焊焊缝的腐蚀产物膜比较致密，只有轻度的皲裂现象。从图 5b 即对应图 5a 的焊缝 C 区

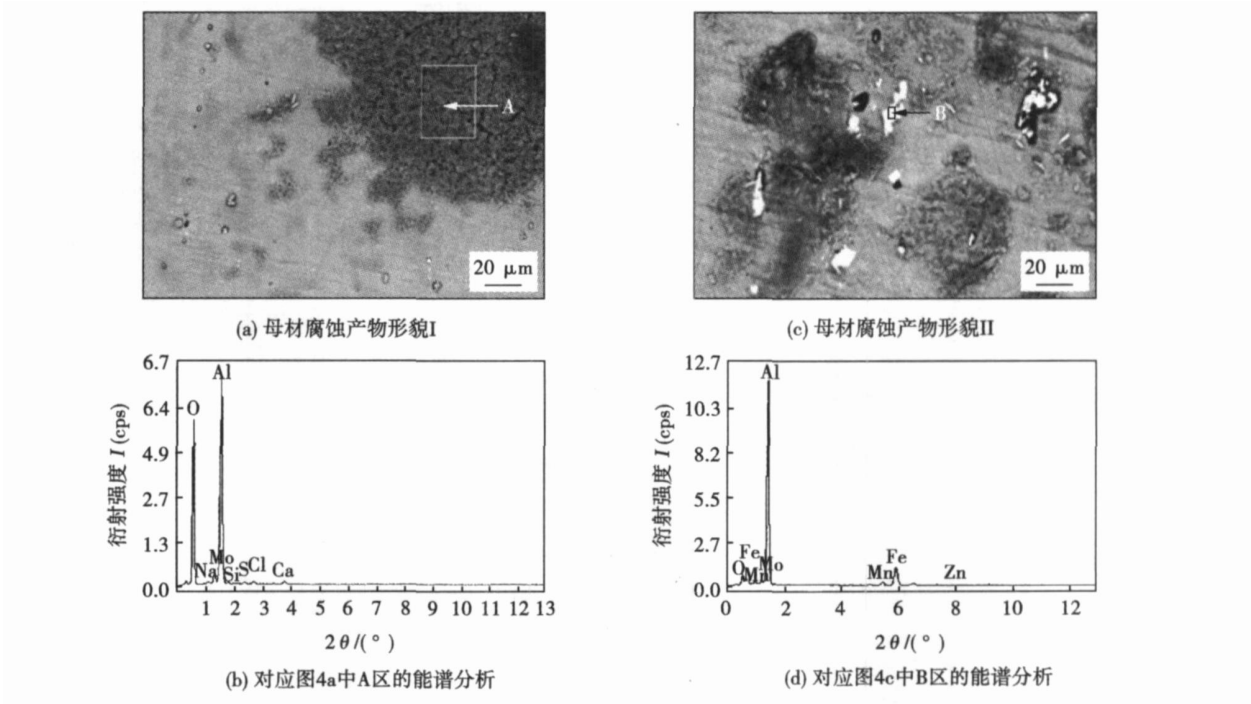

图 4　母材腐蚀产物及能谱分析

Fig. 4　Corrosion products and EDS of base metal

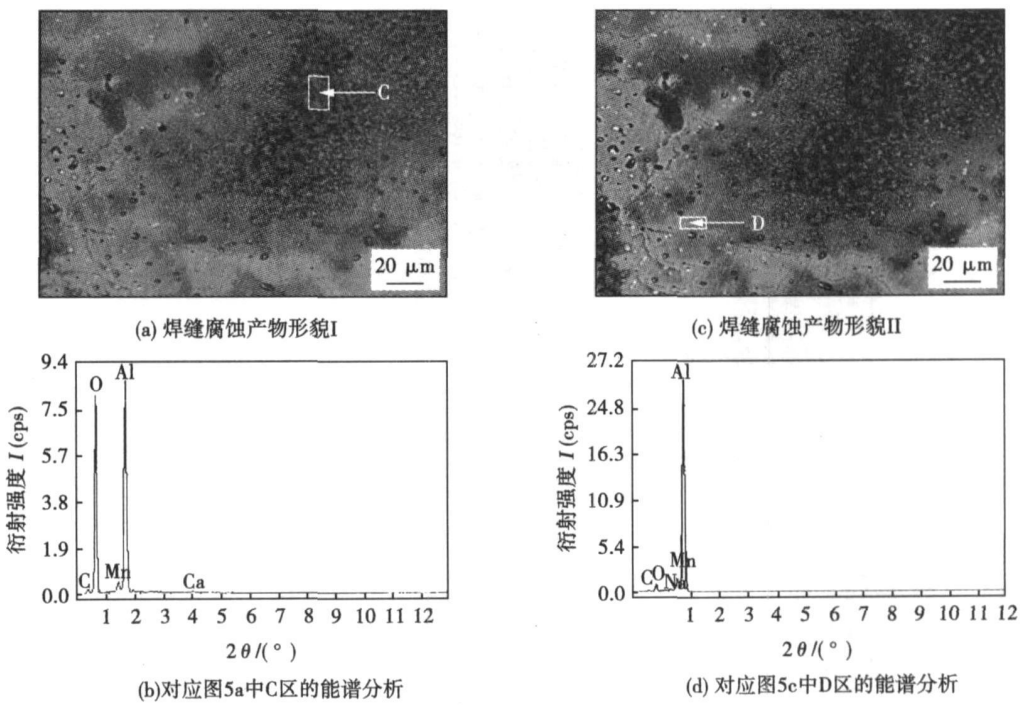

图 5　焊缝腐蚀产物及能谱分析

Fig. 5　Corrosion products and EDS of weld seam

的能谱分析，以及图 5d，即对应图 5c 的焊缝 D 区的能谱分析发现，在焊缝的腐蚀产物中没有 Fe 元素存在。表面双丝焊焊缝耐腐蚀性较好，其耐腐蚀性与其成分有关。所以双丝焊焊缝的腐蚀速度较母材要好。

3　结　　论

（1）通过对板厚为 40 mm 的 7A52 铝合金双丝

焊研究发现,双丝焊焊缝组织均匀致密,焊缝中心形成等轴晶粒。

(2) 7A52 铝合金母材盐雾腐蚀速度较其焊缝要快,表面点腐蚀现象严重,且腐蚀产物膜产生了较严重的皱裂现象。焊缝表面点腐蚀较轻,皱裂现象不明显,焊缝的耐腐蚀性能要优于母材。

参考文献:

[1] 黄兰萍, 陈康华, 李 松, 等. 高温预析出对 Al-Zn-Mg 铝合金组织、力学性能和应力腐蚀性能的影响[J]. 中国有色金属学报, 2005, 15(5): 727-733.

[2] Chen Kanghua, Huang Lanping. Strengthening toughening of 7××× series high strength aluminum alloys by heat treatment[J]. Transactions of Nonferrous Metals Society of China, 2003, 13(3): 484-494.

[3] 张 平, 王卫欣, 赵军军. 7A52 铝合金搅拌摩擦焊接头特征分析[J]. 兵器材料科学与工程, 2004, 27(6): 38-42.

作者简介: 解瑞军, 男, 1969 年出生, 讲师。主要从事金属材料及新材料的焊接研究工作。发表论文 3 篇。

Email: xieruijun7075@163.com

[上接第 56 页]

参考文献:

[1] Zhang Faming, Shen Jun, Sun Jianfei. Processing and properties of carbon nanotubes-nano-WC-Co composites [J]. Materials Science and Engineering A, 2004, 381(1-2): 86-91.

[2] Kear B H, Mccandlish L E. Chemical processing and properties of nanostructured WC-Co materials [J]. Nanostructured Materials, 1993, 3(1-6): 19-30.

[3] Kim B K, Ha G H, Lee G G, *et al*. Structure and properties of nanophase WC/Co/VC/TaC hardmetal [J]. Nanostuctured Materials, 1997, 9(1-8): 233-236.

[4] 赵海锋, 朱丽慧, 马学鸣. 纳米 WC 硬质合金制备新工艺[J]. 材料科学与工程学报, 2003, 21(1): 130-134.

[5] Shipway P H, Mccartney D G. Sliding wear behavior of conventional and nanostructured HVOF sprayed WC-Co coatings [J]. Wear, 2005, 259: 820-827.

[6] Zha Bailin, Wang Hangong, Su Xunjia. Nanostructured WC-12Co coatings sprayed by HVO/AF [C] // Proceedings of the 2004 International thermal spray conference. Osaka, Japan, 2004: 281-284.

[7] 张云乾, 丁彰雄, 范 毅. HVOF 喷涂纳米 WC-12Co 涂层的性能研究[J]. 中国表面工程, 2005, 18(6): 25-29.

[8] Morks M F, Shoeib M A, Brahim A L. Comparative study of nanostructured and conventional WC-Co coatings[C] // Thermal Spray 2004: Advances in Technology and Application. Dusseldorf, German: Verlag fur Schweissen und verwandte Verfahren DVS-Verlag GmbH, 2004: 731-734.

[9] 郭铁波, 周细应, 林文松, 等. 纳米热喷涂技术的研究现状与展望[J]. 表面技术, 2003, 32(4): 1-3.

[10] Yang Q, Senda T, Hiroe A. Sliding wear behavior of WC-12%Co coatings at elevated temperature [J]. Surface & Coatings Technology, 2006, 200: 4208-4212.

[11] Yang Q, Sende T, Ohmorii A. Effect of carbide grain size on microstructure and sliding wear behavior of HVOF-sprayed WC-12%Co coatings [J]. Wear, 2003, 254: 23-34.

[12] Zhao Xiaoqin, Zhou Huidi, Chen Jianmin. Comparative study of the friction and wear behavior of plasma sprayed conventional and nanostructured WC-12%Co coatings on stainless steel [J]. Materials Science and Engineering A, 2006, 431: 290-297.

[13] 李博宇, 董星龙, 刘圆圆, 等. 等离子喷涂法纳米结构 WC-12Co 涂层的微结构与形成机理的研究[J]. 材料工程, 2006, (6): 40-45.

[14] 赵 品, 谢辅洲, 孙振国, 等. 材料科学基础教程[M]. 哈尔滨: 哈尔滨工业大学出版社, 2003.

作者简介: 陈 辉, 男, 1970 年出生, 博士, 副教授, 硕士生导师。主要研究方向为热喷涂、焊接工程技术。发表论文 40 余篇。

Email: xnrpt@163.com

link programs of the hardware driver. The AAES experimental results show that the system not only correctly collects arc voltage, welding current and AAES at high speed synchronously, but also displays the real-time graph of the signals. The whole AAES collecting platform will lay the foundation for further studying on the arc acoustic emission mechanism in the pipe TIG welding.

Key words: pipe welding; arc acoustic emission; LabVIEW

Morphological analysis of interfacial reaction layers in Mo foil and Al foil jointing by diffusion bonding YANG Weihua[1], LI Jinglong[1], XIONG Jiangtao[1], ZHANG Fusheng[1], LÜ Xuechao[2] (1. Shaanxi Key Laboratory of Friction Welding Technologies, Northwestern Polytechnical University, Xi'an 710072, China; 2. China Academy of Engineering Physics, Mianyang 621000, China). p41—45

Abstract: Mo foil and Al foil were joined by diffusion bonding at 600 ℃ and 20 MPa for holding 50 min to 6 h to study the evolvements of the interface reactions at Mo-Al solid-solid interface. The results show that the new phases nucleate and form beneath the Mo substrate skin layer of 0.5—0.7 μm, then teare and lift off the Mo skin, turn to be island-like, and grow into Al substrate with Mo skin sandwiched. Initially, the reaction layers are not plane and like islands distributing along the interface, of which the growing rate is faster in longitudinal than in horizontal; with the islands further growing and joining together, three layers, Mo_3Al_8, $MoAl_5$ and $MoAl_{12}$, arise in sequence from Al-Mo interfacial reaction. When Al element is consumed, $MoAl_4$ phase grows up and forms a new layer between Mo_3Al_8 layer and $MoAl_5$ layer. At last, $MoAl_{12}$ and $MoAl_5$ are consumed and disappear with Mo_3Al_8 layer and $MoAl_4$ layer left on the interface.

Key words: Mo_3Al_8; $MoAl_5$; $MoAl_{12}$; interfacial reaction; diffusion bonding

Weld-softening zone width of 20MnSi controlled cooling bar LIANG Zhifang[1,2], WANG Yingna[1,2], LI Wushen[2], LIU Zhaohui[1], ZHANG Li[1] (1. North China Institute of Science & Technology, Beijing 101601, China; 2. Tianjin University, Tianjin 300072, China). p46—48

Abstract: When the 20MnSi controlled cooling bar is welded, there is a softened zone in the heat affect zone. The softened zone can diminish the load-bearing ability of the bar. By means of controlling the weld process variables and self-temper temperature, the weld-softening zone width can be controlled, and then the load-bearing ability can be improved. The relation model between the self-temper temperature and the welding parameters is gotten and analyzed by using the C.M. Adams formula. The results show that the weld-softening zone width decreases as the self-temper temperature increases, the weld-softening zone widens as the preheating temperature or the heat input increases, and the weld-softening zone of the smaller diameter of bar is wider than that of the bigger diameter of bar.

Key words: controlled cooling; self-temper temperature; heat affect zone; softened zone

Twin microstructure phase and formation mechanisms of aluminized coating ZHANG Wei[1], PANG Bijun[2], ZHANG Jinmin[3] (1. Department of Mechanical and Electrical Engineering, Luoyang Institute of Science and Technology, Luoyang 471023, China; 2. Mathematical Science College, Luoyang Normal University, Luoyang 471022, China; 3. Laboratory of Electron Microscopy, Luoyang Ship Material Research Institute, Luoyang 471039, China). p49—52

Abstract: The La-aluminized coating on 20-carbon-steel was prepared by hot dip aluminizing method. The microstructure of Al_4C_3 phase in the coating was investigated through transmission electron microscope (TEM) after diffusion treatment at 850 ℃ for 4 h. The results indicate that the Al_4C_3 phases are rod-shaped and approximately sphericized, and the twinned Al_4C_3 phases exist in the coating. By using conversion matrix of twin index and the conversion matrix acting on twin index, it is proved that the Al_4C_3 phases are 180° secondary rotation twin with (003) as twinning plane and [001] direction as twinning axis. The long axis direction of rod-shaped Al_4C_3 phases is parallel to (003) plane and perpendicular to [001] direction, and its long axis direction is [210] direction. This shows that there is 180° secondary rotation twin with (003) as twinning plane and [001] direction as twinning axis in hexagonal system. The formation mechanism of the twinned Al_4C_3 phases is also discussed in the paper.

Key words: hot dip aluminizing; diffusion treatment; twin; formation mechanism

Wear behavior of plasma sprayed nanostructured WC-17Co coatings at elevated temperature CHEN Hui[1], GOU Guoqing[1], LIU Yan[1], TU Mingjing[2] (1. Institute of Materials Science and Engineering, Southwest Jiaotong University, Chengdu 610031, China; 2. Institute of Materials Science and Engineering, Sichuan University, Chengdu 610041, China). p53—56, 60

Abstract: Wear is one of main material failure forms. Nanostructured WC-Co coating technology is expected to become a key technology to solve wear-resistance of critical components in large-scale equipments. Nanostructured and ultra-fine WC-17Co coatings were prepared by plasma spraying. The wear behavior at elevated temperature and failure mechanism were investigated. The results indicate that wear resistance at high temperature of the nanostructured WC-17Co coating is much better than that of the ultra-fine coating. The wear mechanism is different between the ultra-fine coating and the nanostructured coating, which low-ductility cracking and abrasive wear following with adhesive wear predominates in ultra-fine coating, and adhesive wear following with abrasive wear predominates in nanostructured coating.

Key words: nanostructured coatings; WC-17Co; elevated temperature wear

Twin-wire welding technology and corrosion resistance of weld seam for 7A52 aluminum alloy XIE Ruijun[1], CHEN Furong[1], ZHANG Chuanchen[1], GAO Yunxi[2] (1. College of Materials Science and Engineering, Inner Mongolia University of Technology, Hohhot

010051, China; 2. Baotou North Engineering Development Co., Ltd, Baotou 014033, China). p57—60

Abstract: The 7A52 aluminum alloys of 40mm in thickness were welded by using Twin-wire gas shielded arc welding (DWGSAW) with ER5356 filler, and the microstructure of the weld seam was analyzed. Meanwhile, according to the actual application environment, the base metal and the weld seam were studied in 3.5% NaCl solution after welding. Results show that the microstructure of the seam welded by DWGSAW is composed of α(Al)+β($MgZn_2$), which the crystal grain is compact and petty, and the center of the weld is equiaxed grain. The corrosion resistance of 7A52 aluminum alloy is liable to pitting corrosion in humid environment containing chloride iron. However, a thin and condense aluminum oxide film is formed on the corroded surface, which is beneficial to increasing the corrosion resistance of the 7A52 aluminum alloy. The corrosion resistance of the weld seam is better and the pitting corrosion is rare on the corroded surface.

Key words: 7A52 aluminum alloy; double-wire gas shielded arc welding; microstructure; corrosion resistance

Solidification crack of SnAgCu lead-free solder joint DONG Wenxing, SHI Yaowu, XIA Zhidong, LEI Yongping, GUO Fu, LI Xiaoyan (School of Materials Science & Engineering, Beijing University of Technology, Beijing 100124, China). p61—63, 68

Abstract: In order to investigate solidification crack of SnAgCu solder joint on the print circuit board (PCB), solidification cracks during solidification are regenerated, the process of the solidification crack formation on the designed specimen is simulated, and the effect of the small element additions on the solidification crack formation of SnAgCu solder joint is researched. Experimental results indicate that some solidification micro-cracks exist significantly on the mini SnAgCu solder joint. The solidification crack susceptibility of Sn-Ag-Cu solder alloy is evaluated by the total crack length of the solder joint, adding trace amounts of Ni and Ce element can depress the solidification crack formation of the solder joints, but adding P element can aggravate the solidification crack formation of SAC305 solder joint and make the crack length evidently increase.

Key words: lead-free solder; SnAgCu solder; solidification crack

Algorithm of weld seam feature detection for remote welding ZHAO Huihui, LIANG Zhimin, GAO Hongming, WU Lin (State Key Laboratory of Advanced Welding Production Technology, Harbin Institute of Technology, Harbin 150001, China). p64—68

Abstract: An algorithm of weld seam feature detection was presented, which was applied to stereo matching of stereo vision system for remote welding. Firstly, the bottom-hat transformation in grey-scale morphology was used to preprocess the image, making the weld seam section more distinctive, and Canny edge detection and close operation were employed to obtain a pixel level closed edge of weld seam; secondly, the edge data was filtered according to continuity and limited width of the weld seam edge; finally, the sub-pixel weld seam edge data was gained by fitting a cubic smoothing spline to the filtered edge data. With the detected sub-pixel weld seam, stereo matching and 3D reconstruction experiments were performed. The results show that the algorithm is rapid, exact and robust to noises.

Key words: remote welding; 3D reconstruction; stereo vision; weld seam feature detection

Effect of relative position of laser beam and arc on formation of weld in laser-MIG hybrid welding GAO Zhiguo, HUANG Jian, LI Yaling, WU Yixiong (Shanghai Key Laboratory of Materials Laser Processing and Modification, Shanghai Jiaotong University, Shanghai 200240, China). p69—73

Abstract: In order to weld high reflectivity aluminum alloy 5083H116 by laser-MIG hybrid welding process, the effects of the front and behind relative position of laser beam and arc on the formation of weld were analyzed. The laser beam incidence angel will seriously affect the weld formation both surface and inside corresponding to different formation mechanism. When the laser beam is in front of the arc in the welding direction, the weld surface is full uniform. While the arc is in front of the laser beam in the welding direction, the inclined trench will appear on the weld surface. With the help of EDX and micro hardness analysis, the Mg content shows a gradual increase from the weld upside surface to the underside surface, but the weld hardness is slight difference. The weld hardness of upside is less than that of underside for the laser beam in front of the arc in the welding direction; the weld hardness of upside is higher than that of underside for the arc in front of laser beam in the welding direction. Meanwhile, there is the black substance on the weld surface after welding, and it is confirmed as oxide of aluminum and magnesium by the EDX.

Key words: aluminum alloy; weld formation; laser-MIG hybrid welding; laser incidence angle

Structure and electrochemistry corrosion behaviors of microarc oxidation on aluminum WANG Zhiping[1], SUN Yubo[1], DING Kunying[1], LIU Jia[1], CAI Xun[2] (1. College of Sciences, Civil Aviation University of China, Tianjin 300300, China; 2. School of Materials Science and Engineering, Shanghai Jiaotong University, Shanghai 200240, China). p74—76

Abstract: The thick, dense and ultra-hard ceramic coating was obtained on the aluminum surface in a silicate electrolyte by microarc oxidation. The surface morphology and cross section of ceramic coating were observed by SEM, the hardness and Young's modulus of ceramic coating were estimated by nano-hardness tester, and the electrochemistry corrosion behaviors of ceramic coating were evaluated using polarization curves. The results show that the highest surface hardness of ceramic surface coating is 25.3 GPa; the hardness and Young's modulus of cross section of coating distribute similarly, both of them decrease from interface to surface of the coating; from the results of electrochemistry, microarc oxidation is effective method to form an anti-corrosion protective film on aluminum.

Key words: aluminum; microarc oxidation; ceramic coating; electrochemistry corrosion behaviors